communications earth & environment

ARTICLE

https://doi.org/10.1038/s43247-022-00490-x OPEN

Anaerobic oxidation has a minor effect on mitigating seafloor methane emissions from gas hydrate dissociation

Christian Stranne [1,2,3]✉, Matt O'Regan [1,2], Wei-Li Hong [1,2,3], Volker Brüchert [1,2], Marcelo Ketzer [4], Brett F. Thornton [1,2] & Martin Jakobsson [1,2]

Continental margin sediments contain large reservoirs of methane stored as gas hydrate. Ocean warming will partly destabilize these reservoirs which may lead to the release of substantial, yet unconstrained, amounts of methane. Anaerobic oxidation of methane is the dominant biogeochemical process to reduce methane flux, estimated to consume 90% of the methane produced in marine sediments today. This process is however neglected in the current projections of seafloor methane release from gas hydrate dissociation. Here, we introduce a fully coupled oxidation module to a hydraulic-thermodynamic-geomechanical hydrate model. Our results show that for seafloor warming rates > 1 °C century^{-1}, the efficiency of anaerobic oxidation of methane in low permeability sediments is poor, reducing the seafloor methane emissions by <5%. The results imply an extremely low mitigating effect of anaerobic oxidation of methane on climate warming-induced seafloor methane emissions.

[1] Department of Geological Sciences, Stockholm University, 106 91 Stockholm, Sweden. [2] Bolin Centre for Climate Research, Stockholm University, Stockholm 106 91, Sweden. [3] Baltic Sea Centre, Stockholm University, Stockholm 106 91, Sweden. [4] Department of biology and environmental science, Linnaeus University, 391 82 Kalmar, Sweden. ✉email: christian.stranne@geo.su.se

Marine sediments along continental margins contain large quantities of methane (CH_4) stored in the structure of solid gas hydrate[1–3]. The stability of CH_4 hydrate in marine sediments is primarily a function of temperature and pressure, and natural gas hydrate deposits are therefore susceptible to destabilization via ocean warming[4–6]. On centennial timescales, climate warming will primarily destabilize the temperature-sensitive feather edge of stability (Fig. 1a) along the upper continental slopes. Although this volume is small compared to the estimated total gas hydrate reservoir[7], large quantities of free CH_4 gas will be mobilized within these sediments during the coming centuries[8,9]. Because CH_4 is a potent greenhouse gas, there is concern that some portion of the mobilized gas will end up in the oceans and potentially the atmosphere where it can reinforce climate warming in a positive feedback loop. Although currently there are only scattered evidence of ongoing hydrate dissociation[10–12], all climate change modeling scenarios predict future widespread hydrate dissociation in response to ocean warming[13–15]. Warming-induced destabilization of natural marine CH_4 hydrate has been proposed as a climate warming mechanism that could exhibit threshold behavior, implying that as climate warming continues this feedback could cause an abrupt transition into a warmer climate state. Although crossing such a threshold is deemed as highly unlikely within the next century[16], this remains a major concern on millennial timescales[4,6,17].

In the context of predicting and quantifying future climate warming-induced seafloor CH_4 release, there remains one major unanswered question—can the anaerobic oxidation of CH_4 (AOM) effectively prevent seafloor gas escape in a warming climate? At present, AOM is the dominant sink consuming more than 90% of the global CH_4 methane production in marine sediments[18–20]. Whether AOM can substantially mitigate climate warming-induced seafloor CH_4 emissions constitutes a formidable knowledge gap that was identified as one of the key future issues in a review by Knittel and Boetius[19], and later raised as one of the key directions for future research by Ruppel and Kessler[21]. In this study, we will only consider sulfate-dependent AOM (hereafter referred to as AOM):

$$CH_4 + SO_4^{2-} \rightarrow HCO_3^- + HS^- + H_2O. \quad (1)$$

The AOM is carried out by a microbial consortium of sulfate-reducing bacteria and methane-oxidizing archaea in a zone where both CH_4 and sulfate are present but are close to depletion. In diffusion-controlled environments this zone appears at the base of the sulfate-reduction zone (SRZ) and is often termed the sulfate-methane-transition (SMT). It is a feature found in all anoxic marine sediments where CH_4 from below and sulfate diffusing down from the seafloor provide energy to the AOM process[19,22,23].

AOM consumes nearly 100% of the methane produced within sediments during diffusive transport towards the seafloor[19,24,25]. It has been hypothesized, however, that a more rapid liberation of CH_4 (in response to climate warming) might lead to fractured pathways within the sediment that bypass the microbial filter thus allowing for a larger proportion of the CH_4 to reach the ocean and potentially the atmosphere[26]. This hypothesis was supported by Stranne et al.[27], who showed that warming-induced hydrate dissociation in moderate- to low-permeability sediments ($k \leq 10^{-16}$ m^2) leads to the formation of hydraulic fractures and rapid release of CH_4 from the seafloor.

Dale et al. [24] argued, however, that in steady state, AOM will consume most of the CH_4 transported from below even in advective systems with large CH_4 transport, implying that AOM would be efficient regardless of the mode of CH_4 transport (advective or diffusive). Their model results point instead to a different mechanism that can allow for substantial quantities of CH_4 to escape from the seafloor: they showed that it will take ~70 years for the microbial biomass to adjust to abruptly changed, higher CH_4 flux conditions. This adjustment period before the AOM community reaches its full capacity represents a "window of opportunity" during which large CH_4 quantities can be released from the seafloor.

Considerable efforts have been dedicated to understand the different aspects of the mechanisms and consequences of CH_4 mobilization in gas hydrate-bearing marine sediments. Reaction-transport models have been applied to investigate the efficiency of the AOM filter e.g.[24,28–30] and the interactions of free gas, dissolved methane, and gas hydrate have been investigated with more advanced multiphase/multicomponent models[14,27,31–33]. Despite these significant advances, constraining the capacity of the microbial filter during warming-induced hydrate dissociation has remained difficult. Reaction-transport models have been applied to assess the efficiency of the AOM filter in a warming-induced hydrate dissociation scenario[24,29], but they used a constant prescribed methane transport into the SRZ and did not consider the dynamics associated with hydrate dissociation. Furthermore, these studies do not account for gaseous CH_4 transport from below that, during gas hydrate dissociation, can account for more than 90% of the total CH_4 transport[14,34].

An important step towards quantifying how much of the mobilized CH_4 gas will escape from the seafloor, and when this

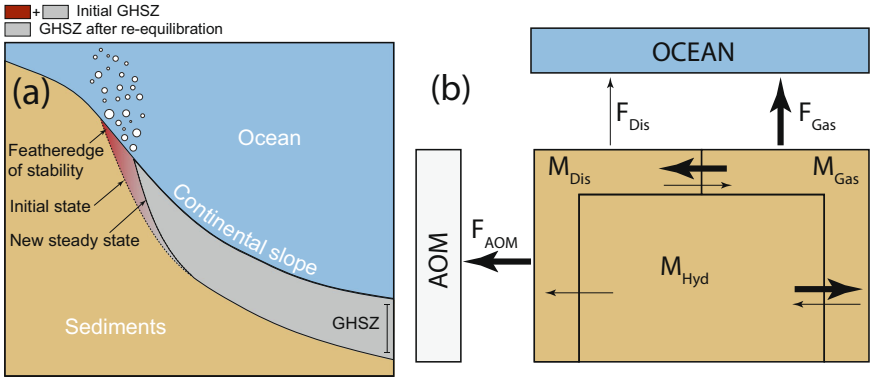

Fig. 1 Schematic view of a shelf slope hydrate system and of the methane (CH_4) transport pathways. a Cartoon of the continental slope and the gas hydrate stability zone (GHSZ) before and after re-equilibration to a warming perturbation of the bottom water. **b** A schematic overview of the three CH_4 mass pools within the sediments and the general direction of the CH_4 mass transport during hydrate dissociation, within and out of the system, illustrated by the thick arrows (minor pathways are indicated by thin arrows).

will occur, involves investigating 1) the rate at which gas hydrates dissociate and 2) the rate at which the mobilized gas can migrate through the sediment and reach the sediment-water interface. Simplified models have been used in the past to make such predictions[8,9,35], but Stranne et al. (2016b) showed that such models can overestimate climate warming-induced seafloor CH_4 emissions by an order of magnitude or more. In order to capture the complexities of a dissociating gas hydrate system, a model needs to consider multiphase fluid- and heat transport and the endothermic reaction of hydrate dissociation. In this study we use a numerical hydrate model TOUGH+Hydrate[36] that considers four mass components (H_2O, CH_4, hydrate and NaCl) partitioned in up to four different phases (gas, liquid, ice and hydrate), coupled with a geomechanical module[27] to account for hydraulic fractures that form in response to overpressure development in low permeability sediments can be accounted for (referred to as T+H-GeoMech hereafter). Stranne et al.[34] added an AOM module to the T+H-GeoMech code, but the approach lacked a dynamic SMT depth (depth was held constant) and had a fixed AOM rate constant (i.e. the maximum AOM capacity of the system was prescribed and held constant). In the present study we build on the model presented in Stranne et al.[34] and by combining results from previous efforts[24,25], we introduce a fully constrained AOM module. The module is fully coupled with the T+H-GeoMech in order to investigate the longstanding question regarding the mitigating effect of AOM on ocean warming-induced seafloor methane emissions. We show that AOM has a minor effect on mitigating seafloor methane emissions from warming-induced gas hydrate dissociation.

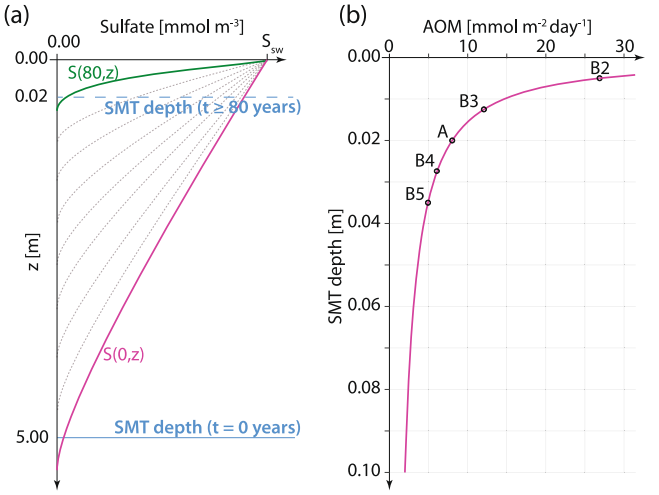

Fig. 2 Vertical sulfate concentration gradient and the corresponding anaerobic oxidation of methane (AOM) capacity. a Schematic view (not to scale) of the transient response of the vertical sulfate profile to a sudden increase in CH_4 flux from below, with inspiration from[24]. S(t,z) is sulfate concentration, t is time in years, and z is depth below seafloor in meters. S_{sw} is the fixed bottom water sulfate concentration and SMT is the sulfate-methane transition at the base of sulfate-reduction zone. **b** The Egger relation[25] describes the depth-integrated AOM capacity as a function of SMT depth. The SMT_{min} for Cases A and B2-B5 are shown as black circles (Case B1 is outside the plotted range).

Results

The migration of the SMT as the control of AOM rates. In the previous effort[34], a rate constant describing the maximum CH_4 oxidation rate from AOM was introduced. This constant was, however, poorly constrained. Furthermore, the SMT did not adjust to changing CH_4 fluxes. It is well known that both the AOM capacity and the SMT depth are functions of CH_4 flux from below[19,25,37]. Here we make use of the empirical relation between AOM capacity and SMT depth presented by Egger et al. (2018, Fig. 2b). The *Egger relation* can be understood as follows. In steady state, there is a balance between the flux of CH_4 into the SRZ from below and the counter flux of sulfate from above (i.e. Equation 1). Here, the ocean is viewed as an infinite source of sulfate with a fixed concentration (i.e. a constant sulfate concentration at the top of SRZ), and the downward sulfate flux from the ocean and into the sediments is diffusive and thus controlled by the vertical sulfate concentration gradient (magenta profile in Fig. 2a). The SMT shallows when the balance is disturbed by a sudden increase in the CH_4 flux from beneath. There are likely two mechanisms leading to the upward movement of the SMT; the advection of sulfate-depleted pore water from below may shoal the SMT mechanically, and microbial biomass growth and sulfate consumption through AOM (enabled by the sudden presence of CH_4) will contribute to depleting the sulfate above the former SMT. With shoaling SMT, the sulfate gradient (and thus diffusive sulfate flux) increases, thus supplying more sulfate for AOM. The SMT shoaling and the subsequent sulfate flux increase continues until a new steady state is reached, where the new perturbed CH_4 flux from below is again balanced by the diffusive sulfate flux from above (green profile in Fig. 2a). In this study, we assume that the SMT depth controls the maximum AOM capacity (through the sulfate gradient) in accordance with[25]. Furthermore, we assume that in non-steady state, the SRZ depth is continuously adjusting to the changing CH_4 fluxes from beneath. The SMT depth (and thus AOM capacity) is thus sluggishly aiming at a moving target, set by the instantaneous CH_4 flux at the SMT, due to the slow response time of microbial growth.

The shallowest SMT depth found in field observations presented in[25] is 3.5 cm. In this study we assume a minimum depth of the SMT (SMT_{min}) of 2 cm in the base case (Case A, Fig. 2b), which, according to the *Egger relation*, corresponds to a maximum depth-integrated AOM rate of about 8 mmol m^{-2} day^{-1}. Orcutt et al.[38] list nine studies from slope sediments (seafloor depths between 200 and 1000 m) all of which reporting depth-integrated AOM rates < 5 mmol m^{-2} day^{-1}. Higher depth-integrated AOM rates have been reported for advective systems (e.g., mud volcanos and cold seeps with thermogenic methane sources), based on observed sulfate profiles (e.g., 16.3 mmol m^{-2} day^{-1}[39]) and ex-situ sulfate-reduction rate analyses (50-140 mmol m^{-2} day^{-1},[40,41]). We therefore performed a sensitivity test with SMT_{min} depths ranging from 0.001 to 0.035 m, corresponding to a maximum AOM capacity in the range 109 to 5 mmol m^{-2} day^{-1} (Case B1-B5, Table 1 and Fig. 2b).

We use the *Egger relation* to calculate the AOM capacity of the system during the re-equilibration phase, under the assumption that the maximum AOM capacity is controlled by the instantaneous sulfate flux (which is set by the SMT depth and the corresponding sulfate gradient). This seems reasonable given that there is an excess of CH_4 during re-equilibration thus rendering a system where AOM is limited by the diffusive sulfate transport from above. However, the *Egger relation* does not provide any information on the rate at which the system is adjusting to new CH_4 flux conditions. A very central question is then: how fast will the microbial biomass build up to its full potential? This question was investigated by Dale et al.[24], with a kinetic–bioenergetic reaction model for AOM. They simulate a diffusive system in steady state with a SMT at 3 mbsf, which is instantaneously transitioned into an advective system with a higher CH_4 flux from beneath. They found that the system reaches a new steady state after 70 years, which represents the time window during which the AOM filter efficiency is limited.

Table 1 Model simulations included in the present study*.

Simulation case	Description
A (base case)	Adjustment time = 80 years, SMT_{min} = 2 cm
B1-B5	Case A with SMT_{min} of 0.1, 0.5, 1.75, 2.75 and 3.5 cm
C1-C2	Case A with adjustment time of 50 and 110 years
D1-D2	Case A with coarser/finer model grid, for k = 10^{-17} m^2
E	AOM module switched off (zero AOM)
F1-F4	Seafloor forcing of 0.0025, 0.005, 0.01 and 0.02 °C $year^{-1}$ (over the first 100 years)

*All model simulation cases listed here are performed over a sediment permeability range of 10^{-17}–10^{-14} m^2 (13 simulations in each case, with a total of 195 simulations).

While the SMT is shoaling, there is an excess of CH_4 within the SRZ and microbial biomass growth is limited by the sulfate flux (set by the SMT depth) and the adjustment time should then be independent of CH_4 flow rates. This idea was corroborated by Date et al[24] who concluded that the 70-year time window reflects the growth kinetics of the AOM community and is essentially independent of the vertical CH_4 flux rate itself. However, the adjustment time scale is subject to uncertainty and may vary depending on e.g. initial conditions and on the reactivity of the organic matter[42,43]. For instance, Treude et al.[44] applied a one-dimensional transport-reaction model with a prescribed methane source injected into initially methane-free sediments to create a non-steady-state SRZ. The authors concluded that reestablishment to steady-state conditions would take 100 years or more. On the other hand, recent estimates of the doubling time of the AOM community (3-9 months[45,46]) suggest shorter adjustment timescales than found by Dale et al.[24] and Treude et al.[44]. Here we assume that the adjustment time is 80 years in the base case (Case A) and we perform a sensitivity test by assigning adjustment times of 50 and 110 years (Cases C1 and C2, Table 1).

AOM efficiency. We show the percentage of pore space occupied by CH_4 gas in the top 20 mbsf (Fig. 3b, d, f), the cumulative seafloor CH_4 flux (blue lines, Fig. 3c, e, g) and cumulative depth-integrated AOM (red lines, Fig. 3c, e, g) for sediments with three different permeabilities under the assigned bottom water warming scenario (Fig. 3a). In the present simulations, the CH_4 transport in lower permeability clay sediments ($k < 10^{-15.5}$ m^2) is completely dominated by flow through hydraulic fractures (for more details, see Stranne et al., 2017). Seafloor CH_4 escape from clay sediments therefore ends abruptly as soon as the hydrate deposit is completely dissociated (about 75 years into the simulation, Fig. 3g) as gas mobilization, pressure build-up, and thus hydraulic fracturing stops at this point. The permeability range of $10^{-15.5} \le k \le 10^{-15}$ m^2 coinciding approximately with (and hereafter referred to as) clayey silt, represents a low-flow regime where porous flow is just large enough for major fracturing not to occur, while at the same time being so small that only limited amounts of gas reaches the seafloor on a centennial time scale (Fig. 3d, e). For higher permeabilities ($k > 10^{-15}$ m^2 silt to clean sand), the porous flow increases steadily with increasing permeability but even in sediments with an intrinsic permeability of 10^{-14} m^2, the seafloor CH_4 emissions are still smaller than for the fracture flow observed in clay sediment (compare Fig. 3c with Fig. 3g). Worth noting in this context is the difference in the quantity of gas that is still lingering within the sediments after 100–200 years (referred to as gas retention, Fig. 3b, d, f) which is highest in the clayey silt, and lowest in the low permeability clay sediments were transport is dominated by fracture flow.

In our simulations, CH_4 begins to migrate into the SRZ about 15 years after the onset of seafloor warming, as manifested by the change in equilibrium SMT depth (blue curve Fig. 4a), and the SMT starts to adjust towards a shallower "high CH_4 flux" equilibrium (red curve Fig. 4a). As the SMT shoals towards the seafloor, the AOM capacity increases logarithmically according to the *Egger relation* (red curve, Fig. 4b). Because the SMT adjustment is not instantaneous, this gives rise to a time window (referred to as a "window of opportunity") during which the CH_4 flux into the SRZ is large while the AOM capacity is still limited, thus resulting in substantial CH_4 bypass through the SRZ and release to the seafloor (blue curve, Fig. 4b). Note that the seafloor gas escape exceeds the depth-integrated AOM rate by more than two orders of magnitude (Fig. 4b). A central question in this study is how efficient the AOM filter is during rapid seafloor warming and subsequent gas hydrate dissociation. The answer depends on the sediment permeability and on how (and when) the efficiency is being evaluated.

We define the AOM filter efficiency as the depth-integrated AOM rate (F_{AOM}) in relation to the total methane supply from below, which is the sum of seafloor CH_4 escape flux (F_{CH4}) and F_{AOM}. This can be described as a percentage

$$\text{AOM filter efficiency}(t) = 100\frac{F_{AOM}(t)}{F_{AOM}(t) + F_{CH_4}(t)} \quad (2)$$

where F_{CH4} is $F_{Gas} + F_{Dis}$ (Fig. 1b). An efficiency of 100% means that all CH_4 entering the SRZ is consumed by AOM and no CH_4 escapes from the seafloor.

Plotting the instantaneous AOM filter efficiency as a function of time (Eq. 2) clearly displays the "window of opportunity" for seafloor CH_4 gas release (blue curve, Fig. 4c). The instantaneous AOM filter efficiency can be somewhat misleading, however, because of the highly variable CH_4 flux through the sediment during these simulations (blue curve, Fig. 4b). Calculating the cumulative AOM filter efficiency (replacing the instantaneous F_{AOM} and F_{CH4} in Eq. 2 with the corresponding cumulative values, or red and blue lines, respectively, from Fig. 2c, e, g) illustrates the relation between the total mass of oxidized CH_4 and total mass of CH_4 escaped from the seafloor at a given time. Such a cumulative expression gives a clearer picture of the total filter efficiency as the system progresses through the different phases of hydrate dissociation and gas migration (red curve, Fig. 4c). The difference between the two measures of filter efficiency is particularly striking in low-permeability clay sediments, where more than 99% of the total CH_4 escape takes place during a period when the efficiency is essentially zero (Fig. 4c). The subsequent CH_4 escape is completely negligible, meaning that the corresponding higher filter efficiency after about 80 years into the simulation has no effect in terms of CH_4 seafloor emissions (compare red and blue curves Fig. 4c).

We summarize how AOM affects seafloor CH_4 emissions for sediments of different permeability in Fig. 5. The cumulative filter efficiency and total CH_4 escape, evaluated after 100 and 200 years are shown in Fig. 5a, c and Fig. 5b, d, respectively. After 100 years, the higher filter efficiency for clayey silts (Fig. 5a) is compensated by relatively low CH_4 fluxes, rendering a negligible effect of AOM on the seafloor CH_4 emissions (compare blue and black curves in

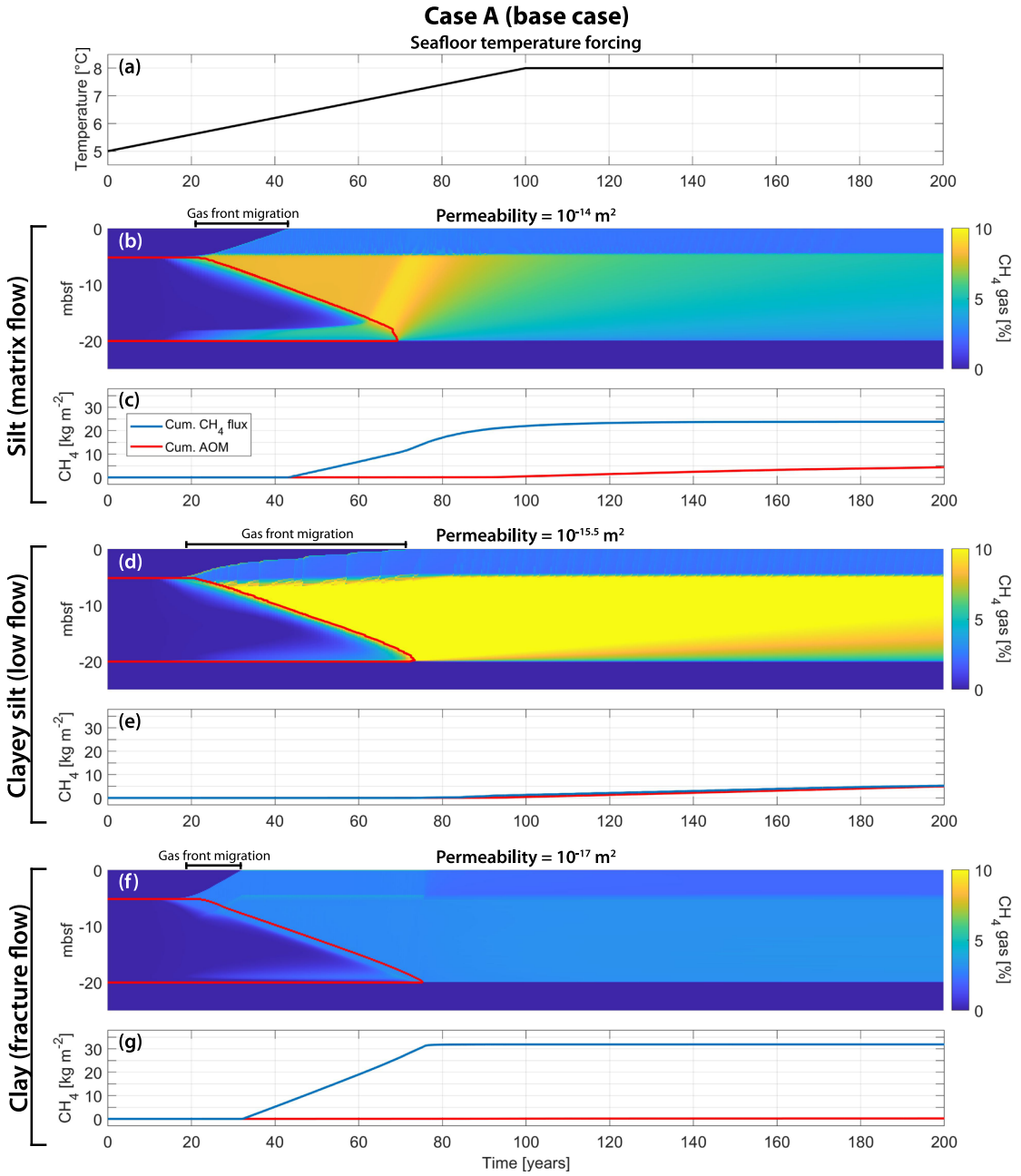

Fig. 3 Simulation results from Case A (base case). a Seafloor temperature forcing. Simulation output for high permeability sediments dominated by matrix flow are shown in (**b**, **c**), medium permeability sediments with comparably low flow are shown in (**d**, **e**) and low permeability sediments dominated by flow through hydraulic fractures are shown in (**f**, **g**). CH_4 gas concentration within the sediment pore space is shown as a function of simulation time (**b**, **d**, **f**) with the red contour marking the depth boundaries of the hydrate deposit thinning with time due to the ongoing hydrate dissociation. Cumulative gas release at the seafloor (solid blue), cumulative AOM (solid red) are shown as functions of time (**c**, **e**, **g**).

Fig. 5b). After 200 years, CH_4 release from low-permeability clay sediments remains largely unaffected by AOM while the higher filter efficiency in clayey silt to clean sand sediments lead to a reduction of the seafloor CH_4 emissions (Fig. 5c, d).

Discussion

Large quantities of CH_4 may be mobilized along the continental slopes in a warming climate scenario due to hydrate dissociation is[8–15]. While AOM is known to function as a highly efficient microbial filter for CH_4 seafloor discharge at present[18–20], it has been speculated that the efficiency might be reduced during climate warming-induced hydrate dissociation due to hydraulic fracturing[26] and due to the slow growth kinetics of the AOM community[24].

Hydrate modeling studies have so far not been able to adequately take AOM into consideration. On the other hand, studies with transport-reaction models[24,29] have not been able to account for gaseous CH_4 transport from below the SMT, nor hydraulic fracturing that results from overpressure development during gas hydrate dissociation. Another limitation of the existing transport-reaction model studies is that the upward transport of CH_4 is prescribed, constant and poorly constrained. These limitations might result in oversimplification of results. For instance, it has been shown that CH_4 transport into the SRZ will be predominantly gaseous, accounting for more than 90% of the total

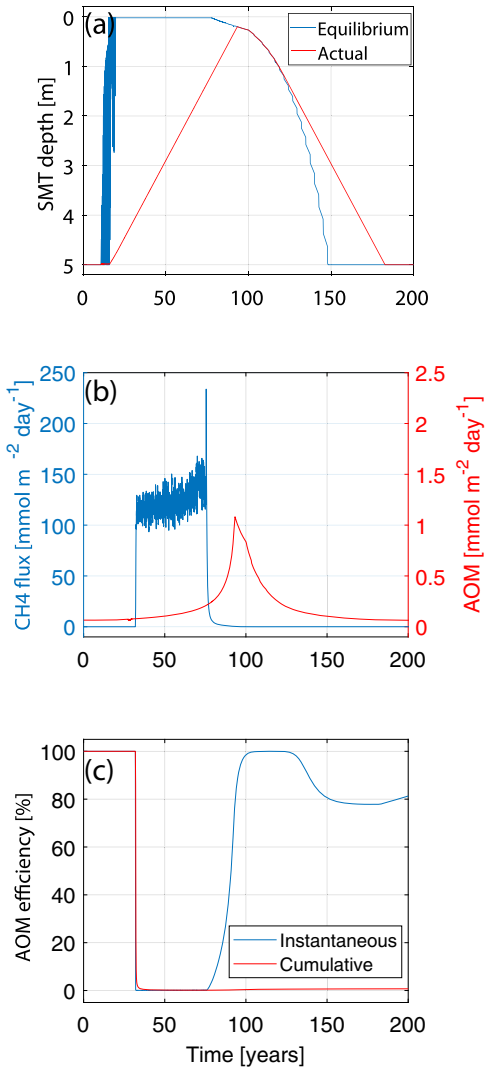

Fig. 4 Model output from Case A with clayey sediments ($k = 10^{-17}$ m^2). **a** The equilibrium/actual depth of the sulfate-methane transition (SMT) (blue/red). **b** CH_4 flux at the seafloor (blue) and anaerobic oxidation of methane (AOM) integrated over the SRZ (red). Note the different scales (two orders of magnitude difference). **c** AOM filter efficiency calculated from instantaneous fluxes (blue) and from the cumulative fluxes (red). Corresponding data for clayey silt ($k = 10^{-15.5}$ m^2) and clean sand ($k = 10^{-14}$ m^2) are shown in Supplementary Fig. 2.

CH_4 transport[14,34]. Furthermore[1], estimate that roughly 90% of global gas hydrate volumes occur in impermeable muds. Stranne et al.[27] showed that in low-permeability sediments (k approximately < $10^{-15.5}$ m^2), close to 100% of CH_4 transport is through hydraulic fractures, implying that this will be the dominant transportation mode of CH_4 during climate warming-induced hydrate dissociation. Lastly, CH_4 transport will not be constant over time during hydrate dissociation, but is expected to vary drastically during the different phases of dissociation and gas migration (and depends strongly on the sediment permeability, Supplementary Fig. 2b, e, h).

In this study we take advantage of one important conclusion of a previous work[24]—the AOM adjustment time reflects the growth kinetics of the AOM community and is essentially independent of the vertical CH_4 flow rate itself. By combining this adjustment time with the assumption that AOM is limited by the diffusive sulfate transport from the overlying ocean water (*Egger relation*), we can study the AOM filter efficiency in a fully coupled and fully constrained numerical geomechanical hydrate model.

Our results suggest that the combination of fast CH_4 migration through the sediments and relatively large CH_4 fluxes leads to an inefficient AOM filter. With the exception of "low-flow" clayey silt sediments, most of the seafloor CH_4 escape occurs before the AOM has reached a new steady state. In clay (silt to clean sand) sediments, more than 99% (90%) of the total CH_4 migration into the SRZ occurs during the first 100 years, with a cumulative AOM efficiency of less than 1% (about 2%) (Fig. 5a). In clayey silt, gas migration is slower and fluxes are more modest. A substantial fraction of the total CH_4 flux migrates, however, into the SRZ after the AOM filter has reached steady state, meaning that the cumulative AOM efficiency is higher. The relatively high cumulative AOM filter efficiency for clayey silts (approaching 50% at $k = 10^{-15.5}$ m^2, Fig. 5b) is compensated by relatively small CH_4 emissions, so that the effect of the AOM on the seafloor CH_4 escape quantities in absolute terms is similar to the higher permeability clean sand sediments with a cumulative efficiency of around 15% (Fig. 5d).

The overall mitigating effect of AOM on seafloor CH_4 release is marginal, regardless of the sediment permeability (Fig. 5b, d). The adjustment time scale and the maximum AOM capacity of the sediments (through the SMT_{min} parameter) are the most critical factors and might, however, be subject to uncertainty. We therefore perform sensitivity analyses on these parameters. The analyses indicate that our model results after 100 years are not sensitive to changes in SMT_{min} (Supplementary Fig. 3a, b, Supplementary Note 1) or adjustment time (Supplementary Fig. 4a, b, Supplementary Note 2). After 200 years, however, the cumulative AOM filter efficiency for clayey silt starts to deviate (Supplementary Figs. 3c, 4c). The higher sensitivity for clayey silt is compensated by generally lower CH_4 flux rates, rendering a fairly small sensitivity in terms of actual seafloor CH_4 release (Supplementary Figs. 3d, 4d). A sensitivity analysis of the grid resolution was also performed (Cases D1-D2, Supplementary Fig. 5, Supplementary Note 3). This analysis shows that, while the frequency of hydraulic fracturing changes with resolution (Supplementary Fig. 5b, e, h), the cumulative seafloor CH_4 emission is not effected (red curves, Supplementary Fig. 5a, d, g).

The seafloor warming rate applied in the base case (0.03 °C year^{-1}) represents a worst case scenario inspired by bottom water temperature observations off Svalbard[12,47]. More moderate warming rates have been observed in e.g. the Antarctic intermediate water[48], presently affecting gas hydrate stability along the Brazilian slope[10]. Climate model predictions of future warming along the continental slopes suggest temperature increases of typically 0.01–0.02 °C year^{-1} over the next 100 years[9,35]. In order to investigate the sensitivity of our results to the seafloor warming rate, we perform a sensitivity study where we apply a warming rate of 0.0025, 0.005, 0.01 and 0.02 °C year^{-1} (Case F14 respectively). Supplementary Figs. 6, 7 show the results of these additional simulations and indicate that the AOM efficiency remains low (< 5% in clay sediments) for simulations with seafloor warming rates ≥ 0.01 °C year^{-1}. The CH_4 discharge in scenarios with seafloor warming rates < 0.01 °C year^{-1} is drastically reduced (e.g. zero CH_4 discharge after 100 years, Supplementary Fig. 6b). These results suggest a threshold in terms of seafloor forcing at 0.005 °C year^{-1}, over which seafloor CH_4 emissions are increased quite drastically (typically well over 100%, Supplementary Fig. 6d). For warming rates < 0.01 °C year^{-1}, the AOM filter does not come into play on the timescales considered in this study due to the corresponding slow dissociation rates. Our results suggest, however, that the cumulative AOM filter efficiencies for these weak seafloor forcing scenarios would become

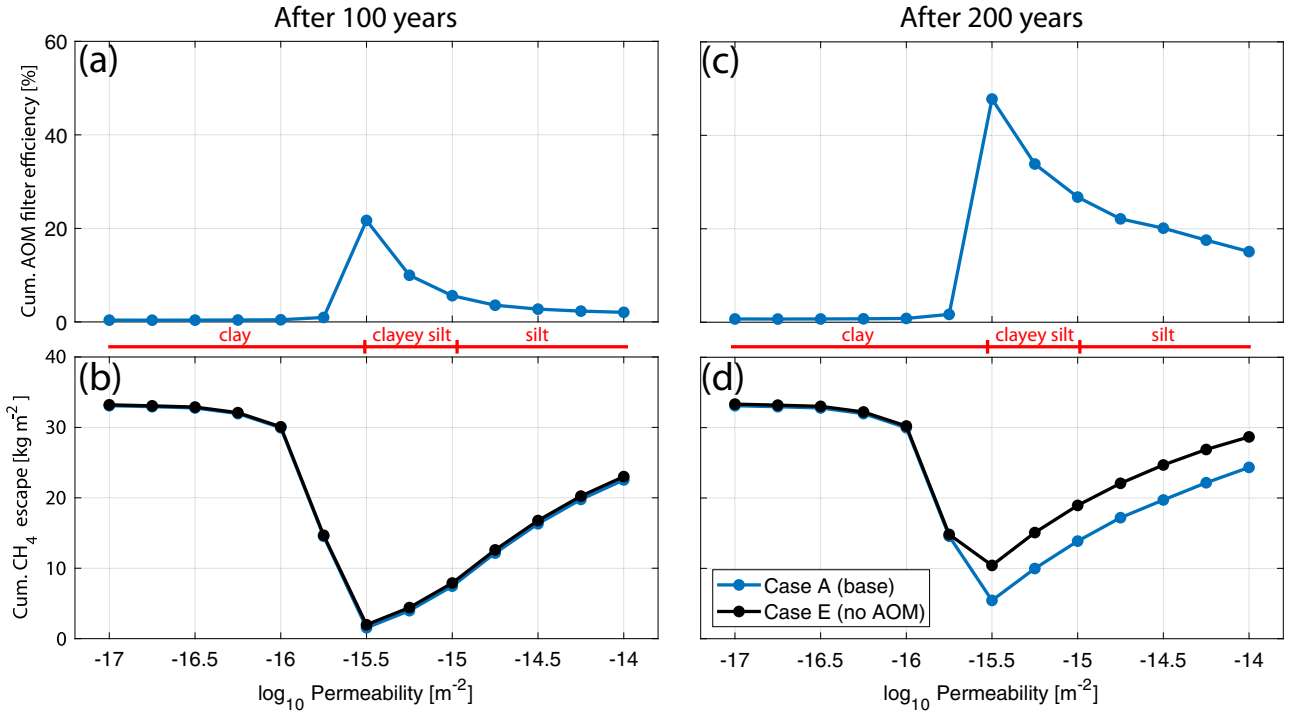

Fig. 5 Summary of modeling results. Model simulation results after 100 years (**a**, **b**) and after 200 years (c-d). Cumulative anaerobic oxidation of methane (AOM) filter efficiency (**a**, **c**) and cumulative gas escape (**b**, **d**) plotted against intrinsic permeability for Case A (baseline, blue) and Case E (no AOM, black). Note that the blue line is essentially hidden behind the black in (**b**), meaning that AOM has a negligible mitigating effect on seafloor emissions over the first 100 years.

more efficient on a millennial time scale as seafloor discharge occurs later, is less intense and cover longer time periods (all of which act to increase the cumulative AOM efficiency). See Supplementary Note 4 for further details.

Dale et al.[24] show seafloor CH_4 release of up to about 5 mmol m^{-2} day^{-1} during equilibration and Puglini et al.[29] report corresponding release of up to around 0.5 mmol m^{-2} day^{-1}, both orders of magnitude smaller than the fluxes reported here (reaching well above 100 mmol m^{-2} day^{-1}, Fig. 4b). The CH_4 fluxes into the SRZ in those studies are prescribed through a constant upward pore water velocity and a constant dissolved CH_4 concentration at the lower boundary. The transport of mobilized free gas into the SRZ in our simulations (not considered in those models) can, at least partly, explain this discrepancy.

The AOM filter efficiencies reported in this study might be overestimated due to the fact that we are not taking the kinetics of CH_4 dissolution into consideration, nor the fact that in reality, CH_4 will tend to become saturated in pore water close to fractures, thus preventing gaseous CH_4 within fractures from dissolving as efficiently as in the present simulations. It has been demonstrated that AOM only consumes a tiny molar fraction (~1‰) of the total CH_4 emissions in places where gas hydrate dissociation is linked to contemporary ocean warming[10]. These results suggest that the AOM filter may be even less efficient than the results presented here. On the other hand, aerobic CH_4 consumption in surficial sediments[49] is not considered in the present study. Furthermore, recent progress on the AOM process indicates that AOM rates may be up to 4 times higher than sulfate-reduction-calculated AOM[50], indicating that electron acceptors other than sulfate can be important, thus increasing the AOM capacity. However, in our sensitivity analysis the maximum AOM capacity is increased by a factor of more than 13, from 8 mmol m^{-2} day^{-1} (Case A) to 109 mmol m^{-2} day^{-1} (Case B1) without any drastic changes of the results, especially not for low permeability sediments where the AOM efficiency remains low (< 1%).

The present study helps determine the fate of future mobilized CH_4 within hydrate-bearing slope sediments, but does not address the fate of the CH_4 once it is emitted to the ocean. If a large fraction of the released CH_4 reaches the atmosphere, this could accelerate climate warming[4,6,17]. If only considering slope hydrate systems (the focus of this study) this appears to be an unlikely scenario. In our simulations, the feather edge of gas hydrate stability is found at around 500 m depth while in colder regions, such as the Arctic Ocean, the gas hydrate stability boundary is found further up on the slope (~300 m depth[15]). Even at these shallower depths, dissolved CH_4 will typically be subject to aerobic oxidation before being mixed up to the surface water where exchange with the atmosphere can occur. Furthermore, direct emissions of gas bubbles will be subject to stripping of CH_4 as the gas within the bubble is replaced by ambient oxygen and nitrogen, and at these seafloor depths, only a small fraction would reach the atmosphere directly[51]. The insights into the interplay of AOM and CH_4 escape from this study also pertain to other settings, however, such as methane-emitting systems associated with subsea permafrost on Arctic continental shelves, where significant portions of the released CH_4 can reach the atmosphere[52,53].

It has been hypothesized that the AOM efficiency might be low during climate warming-induced hydrate dissociation due to hydraulic fracturing[26]. Our results illustrate that hydraulic fracturing is indeed critical for seafloor CH_4 escape dynamics and AOM filter efficiency for two reasons. The first is rather intuitive, as fracturing allows CH_4 to bypass the AOM filter. However, a second important insight from this work is that enhanced gas migration due to fracturing results in a large fraction of CH_4 gas escape before the AOM community reaches its full capacity, i.e. during the "window of opportunity".

Table 2 Physical Properties and T+H-GeoMech Simulation Parameters.

Parameter	Value
Sediment grain density [kg/m^3]	2700[a]
Permeability, k [m^2]	10^{-17} to 10^{-14}
Wet conductivity [W/mK]	1.21[a]
Dry conductivity [W/mK]	0.34[a]
Heat flow [W/m^2]	0.04[b]
Porosity	0.6[a]
Initial seafloor temperature [°C]	5
Seafloor depth [m]	520
Initial hydrate saturation, S_h [%]	5[a]
Initial/boundary pore water salinity [%]	3.5[a]
Gas composition	100% CH_4
Seafloor temperature increase [°C year^{-1}]	0.03 (over first 100 years) [a]
Fracture Permeability [m^2]	10^{-10} [b]
Normalized overpressure threshold	1.0[b]

[a]From ref. [12].
[b]From ref. [27].

Conclusions

In this study we investigate the longstanding question regarding the efficiency of the microbial filter during climate warming-induced hydrate dissociation—will sulfate-dependent AOM in the sediments be able to mitigate the seafloor CH_4 discharge? In the light of the sensitivity analyses performed in the present study, our modeling results are robust and indicate that the mitigating effect of AOM on climate warming-induced seafloor CH_4 escape is minor. The AOM filter becomes particularly inefficient (<5%) when overpressure leads to hydraulic fracturing and rapid CH_4 release, which is expected to be the dominant CH_4 transport mode in hydrate-bearing slope sediments. The underlying reasons are that (1) much of the gas release takes place during AOM re-equilibration during which (2) fluxes are relatively high (order of 100 mmol m^{-2} day^{-1}) and the AOM capacity is limited. The mechanical response of the sediments to overpressure development is faster than the biological response to gas accumulation. These results are valid under scenarios with warming rates ≥ 0.01 °C year^{-1} while below this threshold, the predicted seafloor CH_4 emissions are drastically reduced. Although oxidation of CH_4 within the water column can still be highly effective, the results show that we cannot rely on AOM in marine sediments to mitigate future climate warming-induced seafloor CH_4 emissions.

Method

The T+H code is described in detail in[36] and the geomechanical module GeoMech in[27]. We apply mid-latitude temperature conditions and a seafloor depth of about 520 m below sea level (mbsl), rendering a gas hydrate stability zone (GHSZ) extending from the seafloor and down to 20 m below the seafloor (mbsf). This represents the upper, most temperature-sensitive feather edge of stability although a much larger volume will eventually be affected by the seafloor warming perturbation (Fig. 1a). While it can take thousands of years for gas hydrates in the deep ocean to fully equilibrate[54], gas seepage at the feather edge may occur already about 30 years after the onset of seafloor warming[27]. In the base case (Case A), we simulate the response of the hydrate deposit to a linear increase in seafloor temperature of 3 °C over 100 years. The seafloor temperature is then held constant for the rest of the simulation (a total of 200 years). We also perform a sensitivity test on the seafloor warming rate (Cases F1-4). The hydrate deposit has an initial pore volume saturation of 5% evenly distributed within the GHSZ, and is in thermodynamic equilibrium. The model domain extends to 400 mbsf and consists of 144 grid cells with a size of 0.17 m between 0 and 21 mbsf with a logarithmically increasing grid size between 21 and 400 mbsf. We assume that the upper 5 m of the sediment column is initially within the SRZ and is free of CH_4 hydrate[55], conforming to assumed thicknesses in the previous studies[3,9,12,14,34]. Table 2 summarizes the parameter values used in the model simulations.

Because CH_4 migration under warming-induced hydrate dissociation is a strong function of the intrinsic permeability (k) of the sediments (Stranne et al., 2017), all model simulation scenarios (Table 1) are performed over a sediment permeability range of 10^{-17}–10^{-14} m^2 (a total of 195 simulations), which are typical for clay and silt dominated hemipelagic sediments (Supplementary Fig. 1).

The total CH_4 mass is distributed between three pools in the model domain (Fig. 1b): the hydrate pool ($M_{Hyd}(t,z)$), the gas pool ($M_{Gas}(t,z)$) and the dissolved pool ($M_{Dis}(t,z)$) where t is time and z is the depth below seafloor. Over time, CH_4 can be redistributed between these pools and can be removed from the dissolved pool through AOM within the SRZ ($F_{AOM}(t,z)$), and/or leave the gaseous/dissolved CH_4 pools at the sediment-ocean interface ($F_{Gas}(t)$ and $F_{Dis}(t)$). The $F_{AOM}(t,z)$ is described as a sink only for $M_{Dis}(t,z)$, as gaseous CH_4 is not directly available for the microbes that operate AOM. Nonetheless, AOM also acts as a sink for gaseous CH_4 (i.e. $M_{Gas}(t,z)$) due to the constant reduction in pore water CH_4 concentration by AOM, drawing CH_4 from $M_{Gas}(t,z)$ to $M_{Dis}(t,z)$. In marine sediments, dissolved methane is replenished by in-situ microbial methanogenesis[24]. This process is, however, not included in the current model because the rate of methanogenesis is negligible compared to the amount of CH_4 mobilized through hydrate dissociation[10].

The AOM dynamics are implemented in the model code as follows. In each time step, the *equilibrium SRZ depth* is calculated from the instantaneous CH_4 flux into the SRZ, based on the *Egger relation*. If the *current SRZ depth* is not equal to the *equilibrium SRZ depth*, the system is not in steady state. The *current SRZ depth* is then moving towards equilibrium at a certain rate, based on the adjustment time scale (as discussed below). Meanwhile, the *current SRZ depth* sets the instantaneous AOM capacity of the system.

In our simulations, the CH_4 flux into the SRZ is not constant over the course of the simulations. Thus, the results of[24], where the perturbation in the CH_4 supply is instantaneous and continuous, cannot be directly translated to our simulations. Their results would, however, be applicable to our experimental setup under the assumptions discussed below.

The onset of methane migration into the SRZ is not instantaneous in our experiments, because the heat propagation from overlying bottom waters into the sediments and the subsequent melting of hydrates takes time. Furthermore, we assume that the SRZ depth is constantly adjusting towards the equilibrium depth that is set by the instantaneous CH_4 flux at the SMT. Consequently, the adjustment is halted whenever the elevated CH_4 flux into the SRZ is halted. In order to take the time lag between the onset of seafloor warming and CH_4 migration into the SRZ into account, as well as periods between flux pulses during which adjustment is temporarily halted (or reversed), we translate the adjustment time into a corresponding adjustment speed. This adjustment speed (6.23 cm/year in base Case A) represents the time it would take to re-equilibrate the system to a sudden and continuous CH_4 flux increase, similar to the Dale et al.[24] experiment. Furthermore, we assume that the SMT adjustment speed is the same when the SRZ is expanding as when it is shrinking, meaning that a reduction in biomass due to starvation (lack of CH_4) occurs at the same rate as biomass builds up within the SRZ (when there is a CH_4 surplus). It should be noted, however, that the results are not sensitive to this assumption because the AOM/CH_4 dynamics are mainly determined by the time window just before biomass equilibration, when there is an excess of CH_4 and biomass is increasing.

Data availability

Source data for the figures are available from the Bolin Centre for Climate Research database (https://bolin.su.se/data/stranne-2022-methane-1)[56].

Code availability

The model code can be purchased from Berkeley Lab Marketplace (http://marketplace.lbl.gov, last access: 09 May 2022).

Received: 5 October 2021; Accepted: 29 June 2022;
Published online: 28 July 2022

References

1. Boswell, R. & S. Collett, T. Current perspectives on gas hydrate resources. *Energy Environ. Sci.* **4**, 1206–1215 (2011).
2. Milkov, A. V. Global estimates of hydrate-bound gas in marine sediments: how much is really out there? *Earth-Science Reviews* **66**, 183–197 (2004).
3. Wallmann, K. et al. The Global Inventory of Methane Hydrate in Marine Sediments: a theoretical approach. *Energies* **5**, 2449–2498 (2012).
4. Archer, D., Buffett, B. & Brovkin, V. Ocean methane hydrates as a slow tipping point in the global carbon cycle. *Proc. Natl Acad. Sci.* **106**, 20596–20601 (2009).
5. Nisbet, E. G. Some northern sources of atmospheric methane: production, history, and future implications. *Canadian J. Earth Sci.* **26**, 1603–1611 (1989).
6. Dickens, G. R., O'Neil, J. R., Rea, D. K. & Owen, R. M. Dissociation of oceanic methane hydrate as a cause of the carbon isotope excursion at the end of the Paleocene. https://doi.org/10.1029/95PA02087 (1995).

7. Ruppel, C. D. Methane hydrates and contemporary climate change. *Nat. Educ. Knowl.* **3**, 29 (2011).
8. Hunter, S. J., Goldobin, D. S., Haywood, A. M., Ridgwell, A. & Rees, J. G. Sensitivity of the global submarine hydrate inventory to scenarios of future climate change. *Earth Planet. Sci. Lett.* **367**, 105–115 (2013).
9. Kretschmer, K., Biastoch, A., Rüpke, L. & Burwicz, E. Modeling the fate of methane hydrates under global warming. *Global Biogeochem. Cycles* 2014GB005011 https://doi.org/10.1002/2014GB005011 (2015).
10. Ketzer, M. et al. Gas hydrate dissociation linked to contemporary ocean warming in the southern hemisphere. *Nat. Commun.* **11**, 3788 (2020).
11. Phrampus, B. J., Hornbach, M. J., Ruppel, C. D. & Hart, P. E. Widespread gas hydrate instability on the upper U.S. Beaufort margin. *J. Geophys. Res. Solid Earth* **119**, 2014JB011290 (2014).
12. Thatcher, K. E., Westbrook, G. K., Sarkar, S. & Minshull, T. A. Methane release from warming-induced hydrate dissociation in the West Svalbard continental margin: Timing, rates, and geological controls. *J. Geophys. Res. Solid Earth* **118**, 22–38 (2013).
13. Milkov, A. V. & Sassen, R. Two-dimensional modeling of gas hydrate decomposition in the northwestern Gulf of Mexico: significance to global change assessment. *Global Planet. Change* **36**, 31–46 (2003).
14. Reagan, M. T. & Moridis, G. J. Dynamic response of oceanic hydrate deposits to ocean temperature change. *J. Geophys. Res.* **113**, C12023 (2008).
15. Stranne, C. et al. Dynamic simulations of potential methane release from East Siberian continental slope sediments. *Geochem. Geophys. Geosyst.* **17**, 872–886 (2016).
16. Stocker, T. F. et al. *IPCC, 2013: Climate Change 2013: the Physical Science Basis. Contribution of Working Group I to the Fifth Assessment Report of the Intergovernmental Panel on Climate Change* (IPCC, 2013).
17. Kennett, J. P., Cannariato, K. G., Hendy, I. L. & Behl, R. J. Carbon isotopic evidence for methane hydrate instability during quaternary interstadials. *Science* **288**, 128–133 (2000).
18. Hinrichs, K.-U. & Boetius, A. in *Ocean Margin Systems* (eds. Wefer, P. D. G. et al.) 457–477 (Springer, 2002).
19. Knittel, K. & Boetius, A. Anaerobic oxidation of methane: progress with an unknown process. *Annu. Rev. Microbiol.* **63**, 311–334 (2009).
20. Reeburgh, W. S. Oceanic methane biogeochemistry. *Chem. Rev.* **107**, 486–513 (2007).
21. Ruppel, C. D. & Kessler, J. D. The interaction of climate change and methane hydrates. *Rev. Geophys.* **55**, 2016RG000534 (2017).
22. Barnes, R. O. & Goldberg, E. D. Methane production and consumption in anoxic marine sediments. *Geology* **4**, 297–300 (1976).
23. Malinverno, A. & Pohlman, J. W. Modeling sulfate reduction in methane hydrate-bearing continental margin sediments: Does a sulfate-methane transition require anaerobic oxidation of methane? *Geochem. Geophys. Geosyst.* **12**, Q07006 (2011).
24. Dale, A. W., Van Cappellen, P., Aguilera, D. R. & Regnier, P. Methane efflux from marine sediments in passive and active margins: estimations from bioenergetic reaction–transport simulations. *Earth Planet. Sci. Lett.* **265**, 329–344 (2008).
25. Egger, M., Riedinger, N., Mogollón, J. M. & Jørgensen, B. B. Global diffusive fluxes of methane in marine sediments. *Nat. Geosci.* **11**, 421–425 (2018).
26. Buffett, B. & Archer, D. Global inventory of methane clathrate: sensitivity to changes in the deep ocean. *Earth Planet. Sci. Lett.* **227**, 185–199 (2004).
27. Stranne, C., O'Regan, M. & Jakobsson, M. Modeling fracture propagation and seafloor gas release during seafloor warming-induced hydrate dissociation. *Geophys. Res. Lett.* **44**, 8510–8519 (2017).
28. Hong, W.-L., Torres, M. E., Kim, J.-H., Choi, J. & Bahk, J.-J. Towards quantifying the reaction network around the sulfate–methane-transition-zone in the Ulleung Basin, East Sea, with a kinetic modeling approach. *Geochim. Cosmochim. Acta* **140**, 127–141 (2014).
29. Puglini, M., Brovkin, V., Regnier, P. & Arndt, S. Assessing the potential for non-turbulent methane escape from the East Siberian Arctic Shelf. *Biogeosciences* **17**, 3247–3275 (2020).
30. Sauer, S. et al. Methane transport and sources in an Arctic deep-water cold seep offshore NW Svalbard (Vestnesa Ridge, 79°N). *Deep Sea Res. Part I: Oceanogr. Res. Papers* **167**, 103430 (2021).
31. Darnell, K. N. & Flemings, P. B. Transient seafloor venting on continental slopes from warming-induced methane hydrate dissociation: transient seafloor venting from hydrates. *Geophys. Res. Lett.* **42**, 10,765–10,772 (2015).
32. Liu, X. & Flemings, P. B. Dynamic multiphase flow model of hydrate formation in marine sediments. *J. Geophys. Res.* **112**, B03101 (2007).
33. Stranne, C., O'Regan, M. & Jakobsson, M. Overestimating climate warming-induced methane gas escape from the seafloor by neglecting multiphase flow dynamics. *Geophys. Res. Lett.* **43**, 8703–8712 (2016).
34. Stranne, C., O'Regan, M., Jakobsson, M., Brüchert, V. & Ketzer, M. Can anaerobic oxidation of methane prevent seafloor gas escape in a warming climate? *Solid Earth* **10**, 1541–1554 (2019).
35. Biastoch, A. et al. Rising Arctic Ocean temperatures cause gas hydrate destabilization and ocean acidification. *Geophys. Res. Lett.* **38**, L08602 (2011).
36. Moridis, G. J. TOUGH+HYDRATE v1.2 User's Manual: A Code for the Simulation of System Behavior in Hydrate-Bearing Geologic Media. *eScholarship* (2014).
37. Borowski, W. S., Paull, C. K. & Ussler, W. Marine pore-water sulfate profiles indicate in situ methane flux from underlying gas hydrate. *Geology* **24**, 655–658 (1996).
38. Orcutt, B. N., Sylvan, J. B., Knab, N. J. & Edwards, K. J. Microbial ecology of the Dark Ocean above, at, and below the Seafloor. *Microbiol. Mol. Biol. Rev.* **75**, 361–422 (2011).
39. Haese, R. R., Meile, C., Van Cappellen, P. & De Lange, G. J. Carbon geochemistry of cold seeps: Methane fluxes and transformation in sediments from Kazan mud volcano, eastern Mediterranean Sea. *Earth. Planet. Sci. Lett.* **212**, 361–375 (2003).
40. Boetius, A. et al. A marine microbial consortium apparently mediating anaerobic oxidation of methane. *Nature* **407**, 623–626 (2000).
41. Treude, T., Boetius, A., Knittel, K., Wallmann, K. & Jørgensen, B. B. Anaerobic oxidation of methane above gas hydrates at Hydrate Ridge, NE Pacific Ocean. *Marine Ecol. Prog. Ser.* **264**, 1–14 (2003).
42. Meister, P., Liu, B., Ferdelman, T. G., Jørgensen, B. B. & Khalili, A. Control of sulphate and methane distributions in marine sediments by organic matter reactivity. *Geochim. Cosmochim. Acta* **104**, 183–193 (2013).
43. Regnier, P. et al. Quantitative analysis of anaerobic oxidation of methane (AOM) in marine sediments: a modeling perspective. *Earth-Sci. Rev.* **106**, 105–130 (2011).
44. Treude, T. et al. Biogeochemical consequences of nonvertical methane transport in sediment offshore Northwestern Svalbard. *J. Geophy. Res.: Biogeosciences* **125**, e2019JG005371 (2020).
45. Ruff, S. E. et al. In situ development of a methanotrophic microbiome in deep-sea sediments. *ISME J* **13**, 197–213 (2019).
46. Klasek, S. et al. Microbial communities from Arctic marine sediments respond slowly to methane addition during ex situ enrichments. *Environ. Microbiol.* **22**, 1829–1846 (2020).
47. Westbrook, G. K. et al. Escape of methane gas from the seabed along the West Spitsbergen continental margin. *Geophys. Res. Lett.* **36**, (2009).
48. Schmidtko, S. & Johnson, G. C. Multidecadal warming and shoaling of Antarctic intermediate water. *J. Climate* **25**, 207–221 (2012).
49. Boetius, A. & Wenzhöfer, F. Seafloor oxygen consumption fuelled by methane from cold seeps. *Nat. Geosci.* **6**, 725–734 (2013).
50. Bowles, M. W. et al. Remarkable capacity for anaerobic oxidation of methane at high methane concentration. *Geophys. Res. Lett.* **46**, 12192–12201 (2019).
51. McGinnis, D. F., Greinert, J., Artemov, Y., Beaubien, S. E. & Wüest, A. Fate of rising methane bubbles in stratified waters: How much methane reaches the atmosphere? *J. Geophys. Res.* **111**, C09007 (2006).
52. Shakhova, N. et al. Extensive methane venting to the atmosphere from sediments of the East Siberian Arctic Shelf. *Science* https://doi.org/10.1126/science.1182221 (2010).
53. Thornton, B. F., Geibel, M. C., Crill, P. M., Humborg, C. & Mörth, C.-M. Methane fluxes from the sea to the atmosphere across the Siberian shelf seas. *Geophys. Res. Lett.* **43**, 5869–5877 (2016).
54. Archer, D. Methane hydrate stability and anthropogenic climate change. *Biogeosciences* **4**, 521–544 (2007).
55. Bhatnagar, G. et al. Analytical theory relating the depth of the sulfate-methane transition to gas hydrate distribution and saturation. *Geochem. Geophys. Geosyst.* **12**, Q03003 (2011).
56. Stranne, C. Selected model output from numerical simulations of future climate warming-induced seafloor methane escape. *Bolin Centre Database* Dataset version 1.0 https://doi.org/10.17043/stranne-2022-methane-1 (2022).

Acknowledgements

C.S. received support from the Swedish Research Council (VR; grant 2018-04350), M.O. received support from the Swedish Research Council (VR; grant 2020-04379) and M.J. received support from the Swedish Research Council (VR; grant number 2021-04512).

Author contributions

C.S. conceived the original idea of the paper, wrote and integrated the AOM code into the T+H model, and performed the model simulations. All other authors (M.O., W-L.H., V.B., M.K., B.T., and M.J.) have helped with the interpretation of the modeling results, and in revising the manuscript.

Funding

Open access funding provided by Stockholm University.

Competing interests

The authors declare no competing interests.

Additional information

Supplementary information The online version contains supplementary material available at https://doi.org/10.1038/s43247-022-00490-x.

Correspondence and requests for materials should be addressed to Christian Stranne.

Peer review information *Communications Earth & Environment* thanks the anonymous reviewers for their contribution to the peer review of this work. Primary Handling Editors: Mojtaba Fakhraee and Clare Davis. Peer reviewer reports are available.